Colossal dielectric and magnetodielectric effect in Er_2O_3 nanoparticles embedded in a SiO_2 glass matrix

S. Mukherjee, C. H. Chen, C. C. Chou, K. F. Tseng, B. K. Chaudhuri,* and H. D. Yang†
Department of Physics and Center for Nanoscience and Nanotechnology, National Sun Yat-Sen University, Kaohsiung 804, Taiwan
(Received 1 March 2010; revised manuscript received 26 June 2010; published 10 September 2010)

An intriguing colossal enhancement of dielectric constant along with magnetodielectric (MD) behavior is observed in nanoparticle (NP) Er_2O_3 (0.5 mol %) embedded SiO_2 glass matrix synthesized via sol-gel route. A broad dielectric peak with a maximum at T_m (~270 K) exhibits typical diffuse phase transition following modified Curie-Weiss behavior. Conduction mechanism (showing energy barrier $E_a \sim 1.13$ eV near T_m) is closely related to the thermally activated oxygen vacancies. At the highest applied magnetic field 9 T, the dielectric constant around T_m is enhanced almost ~2.75 (at 2.5 kHz frequency) times compared with that at zero field. The MD effect observed in this glassy composite is considered to be associated with the direct consequence of magnetoresistance changes which depends on the magnetic NP size and separation.

DOI: 10.1103/PhysRevB.82.104107 PACS number(s): 77.55.Nv, 77.80.bn, 85.30.Tv

I. INTRODUCTION

Recent urge of device miniaturization has encouraged many researchers[1,2] worldwide for the development of new class of high-k materials in which their dielectric constant could be modified by application of both electric and magnetic field. But relatively few highly prospective compounds have so far been developed showing magnetodielectric (MD) effect around room temperature. Multiferroic $BiMnO_3$ or $BiFeO_3$ based perovskites and their films are very promising materials.[3,4] However, the synthesis and crystallochemistry of Bi- and Mn-based perovskites are quite complex, and the stabilization of the pure phase and accurate control of its composition and oxygen stoichiometry also pause some additional problems.[5,6] Similarly various oxides such as HfO_2,[7,8] ZrO_2,[9,10] TiO_2,[11] Al_2O_3,[12] La_2O_3,[13] Pr_2O_3,[14] etc., have also been studied to find a suitable replacement of SiO_2, as the thickness of SiO_2 gate films in metal-oxide semiconductor field effect transistor devices has almost reached the quantum tunneling limit ~1.5–2.5 nm. Currently intensive research has been focused on amorphous oxide material.[15] However, most of the amorphous high-k oxides of recent development are polycrystalline at the high temperature wherein grain-boundary effect leads to high leakage current.[16] Therefore, the exploitation of prospective amorphous high-k material with superior phase stability is still an open challenge to researchers. It is, therefore, highly desirable to design and synthesize multifunctional materials that operate around room temperature.

Recently, there has been a trend of development of magnetic nanoparticle (NP) in nonmagnetic dielectric matrix to tailor desired magnetic, dielectric, and other properties depending on the concentration of the magnetic ions.[17] Several authors have reported MD response in magnetic NPs systems with a variety of complex mixed perovskites.[18,19] However, these types of perovskites possess compositional variations, structural inhomogeneities, or phase heterogeneities in physical scale from micron or submicron range to the atomic level. This suggests that the high-k value and MD behavior of aforementioned complex system is not a fundamental property but is rather an artifact associated with mesoscopic heterogeneities of the system. Therefore, searching for alternative materials containing single-valent ions with phase stability would be highly desirable. In this article, we have attempted to make superparamagnetic[20] Er_2O_3 NPs embedded in SiO_2 glass matrix by adopting a sol-gel method. We have used sol-gel process because it provides a convenient way for tailoring phase pure, self-organized Er_2O_3 NPs of nearly uniform sizes and for facilitating homogeneous dispersion of these metal-oxide NPs in the silica matrix. In the present work, rare-earth Er_2O_3 magnetic oxide NPs have been grown with diluted concentration in inorganic silica matrix. Interestingly, this glassy system shows colossal enhancement of dielectric constant along with interesting MD effect. Among various rare-earth oxides, Er_2O_3 has been chosen as it possess most appealing properties viz. high resistivity (10^{12}–10^{15} cm^{-3}), large band gap (E_g=5–7 eV), static dielectric constant ($k \sim 14$),[21,22] good thermodynamic stability with silicon and, moreover, not yet been explored from the view point of observing the high MD effect.

II. EXPERIMENTAL DETAILS

The Er_2O_3:SiO_2 NP-glass composite system was synthesized by sol-gel process under atmospheric conditions and at moderate temperature. Erbium-oxide-doped silica gel was prepared from tetraethylorthosilicate (TEOS) and dopant erbium chloride having optimum amount of 0.5 mol % dopant concentration. The method is based on the hydrolysis of precursors (TEOS) and subsequent condensation of hydrolyzed TEOS in a medium containing a hydroalcoholic solution of erbium salt as described elsewhere.[23] The sol-gel derived dried monolithic transparent gel samples were calcined at different temperatures 700, 800, 900, and 1200 °C (henceforth referred as Er05–7, Er05–8, Er05–9, and Er05–12, respectively), in accordance with preselected temperature schedule.[23]

It is found that the erbium chloride doped silica glass prepared by the sol-gel process becomes porous when calcined at ~400 °C and that the pores start to collapse around ~700 °C similar to the pure silica gel glass.[24] With increasing temperature, ≡Si—OH groups condense to

≡Si—O—Si≡ bonds and thus enhancing pore collapse, isolated metal-oxide ions loosely attached to the pores are detached to form clusters. The dimensions of the clusters reside in the nanometer range depending on the annealing temperature. At higher temperature, namely, 800 °C, collapse of larger pores also takes place, agglomerate more Er_2O_3 to form bigger size NP.[25] Thus at the highest temperature employed in the present case, i.e., 1200 °C, Er_2O_3 NPs grow to biggest sizes as observed from x-ray diffraction (XRD) and transmission electron microscopy (TEM) studies.

For characterization, powder XRD of the sample was performed by using Cu $K\alpha$ radiation. An ultrahigh-resolution TEM (Model: JEM-3010, JEOL) was employed to analyze the detailed structure of Er05–7 and Er05–8 samples. The MD measurements were carried out with LCR meter (Model E4980A, Agilant) in conjunction with laboratory built cryostatic arrangement[26] integrated to the physical properties measurement system (Model: 6000, Quantum Design) configured up to 9 T magnetic field. Ferroelectric hysteresis loop was detected by using a Precision LC meter (Model: 609E-6, Radiant Technologies). In this paper, we concentrate the variations in temperature and frequency dependent MD properties mainly on the Er05–8 sample for clarity and compare the analysis with Er05–7, Er05–9, and Er05–12 samples.

III. RESULTS AND DISCUSSION

A. Sample characterization by TEM and XRD

The TEM image of the powder specimen Er05–8 [Fig. 1(a)] shows nearly spherical NPs of Er_2O_3 in the range of 3–6 nm embedded in the glass matrix. The particle size distributions histogram [upper inset of Fig. 1(a)] of the sample is calculated from Fig. 1 shown in Table I. Representative high-resolution TEM (HRTEM) image [lower inset of Fig. 1(a)] of the Er_2O_3 NPs of the respective sample also shows lattice fringes with interplanar spacing (3.04 Å). The selected-area electron-diffraction pattern shows spotted ring patterns suggesting development of regions of localized crystallinity [Fig. 1(b)]. The XRD patterns of the high-temperature annealed system Er05–12 become crystalline with quite large Er_2O_3 NPs (>40 nm). There clearly exhibits [Fig. 1(c)] the most intense characteristic line corresponding to the single phase Er_2O_3 (Ref. 27) at $2\theta \sim 29.30°$ (222) with the refined unit-cell parameter $a=10.54$ Å [space group: $Ia3$ (206)]. Applying the well-known Scherrer's equation, sizes of Er-oxide NPs (Er05–12) are also estimated from the integral breadths of the lines as shown in Table I. The XRD patterns of Er05–7 and Er05–8 samples cannot be well resolved due to their amorphouslike character. Only a very feeble broad peak can be traced with great difficulty in the XRD domain, $2\theta=10°-65°$. It is confirmed that the sizes of Er_2O_3 NPs embedded in the silica glass matrix grow larger for samples calcined at higher temperatures.

B. Temperature and frequency dependence of dielectric response

Figure 2(a) illustrates temperature-dependent real part of the relative dielectric constant (ε') of the Er05–8 sample in

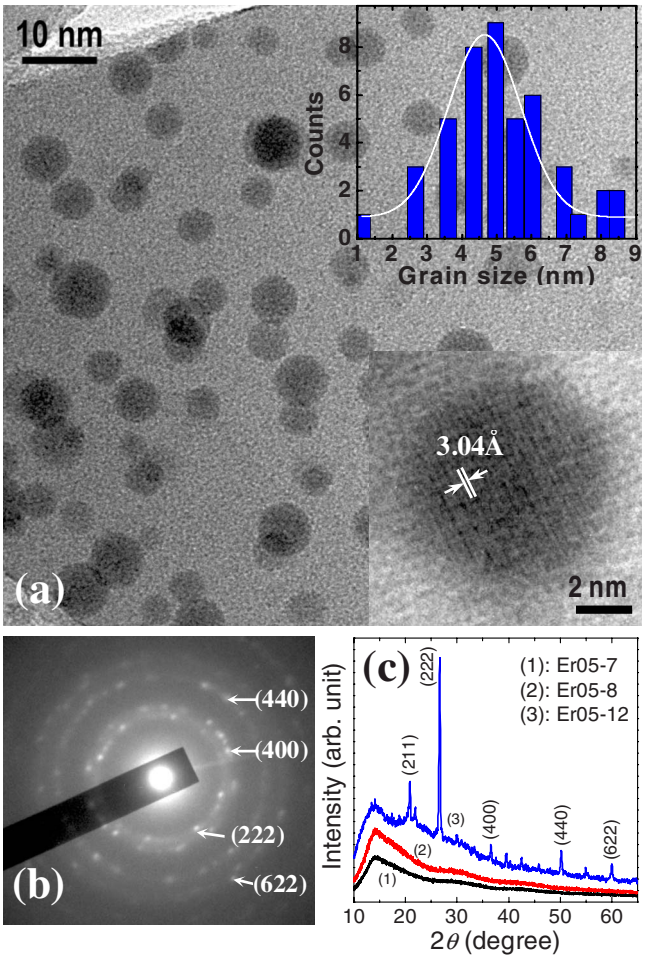

FIG. 1. (Color online) (a) TEM image of Er05–8, upper inset: the particle size distribution histogram and lower inset: the HRTEM image, (b) Electron diffraction, and (c) XRD patterns of all the samples (Er05–7 and Er05–8 showing amorphouslike character).

the absence of magnetic field measured at several selective frequencies (1–100 kHz). The curves show well-defined maxima at $T_m \sim 270$ K. However, such a notable dielectric broadening around ε'_m (maximum value of ε') is indicative of a diffuse phase transition (DPT) (Refs. 28–30) with high ε' (~600 at 1 kHz), quite different from and much higher than that of pure bulk Er_2O_3 ($\varepsilon' \sim 11.5$) (Ref. 31) and SiO_2 ($\varepsilon' \sim 3.9$). Following the concept of DPT, the dielectric constant accords with a modified Curie-Weiss-type equation viz. $\varepsilon'^{-1}-\varepsilon'^{-1}_m = C_i(T-T_m)^\gamma$, where γ is the diffuseness exponent indicative of degree of disorder, C_i is a temperature independent coefficient (in general, dependent of frequency) and ε'_m is the maximum value of ε' at T_m. For $\gamma=1$, it is a normal Curie-Weiss behavior and for $\gamma \sim 2$, it generally implies typical DPT for the ideal ferroelectric relaxor.[32] In the inset of Fig. 2(a), representative plots of $\ln(\varepsilon'^{-1}-\varepsilon'^{-1}_m)$ vs $\ln(T-T_m)$ at several different frequencies are illustrated. A linear fitting for the present Er05–8 system, we obtained average $\gamma = 1.84$ from different slopes, which is close to the relaxor value observed in several oxide relaxors.[33] The space charge or interfacial polarization may be operative in this specimen at temperature above T_m. However, the high ε' is observed even at temperature below T_m (~250–260 K) which indi-

TABLE I. Powder XRD and TEM structural data and other parameters of the MD Er_2O_3:SiO_2 NP-glass composite samples.

Sample	Crystallinity and particle size (from XRD) (nm)	Particle size (from TEM) (nm)	Curie-Weiss fitting parameters		
			Field (T)	$T_\circ$ (K)	C (K)
Er05–7	Predominantly amorphous	≈2			
Er05–8	Predominantly amorphous	≈5	0	260.06	3968.82
			5	270.12	6211.29
			9	271.64	6918.04
Er05–12	>40				

cates that any space charge or interfacial polarization is not quite responsible for the enhancement of dielectric constant below T_m. The ε' value along with DPT behavior [Fig. 2(b)] diminishes with increasing calcination temperature, i.e., the Er_2O_3 NP size. It is worthwhile to mention that the temperature and frequency dependent ε' of the corresponding higher temperature (1200 °C) calcined Er05–12 crystalline sample [inset of Fig. 2(b)] does not show this interesting DPT behavior, similar to pure bulk Er_2O_3 (Ref. 31) or SiO_2. The critical calcination temperature above which DPT behavior completely diminishes for this typical concentration of Er_2O_3 (~0.5 mol %) is found to be around 1000 °C. The DPT behavior is thus confined to the low-temperature calcined (<1000 °C) system only where the amorphous NPs are in the 2–10 nm range.

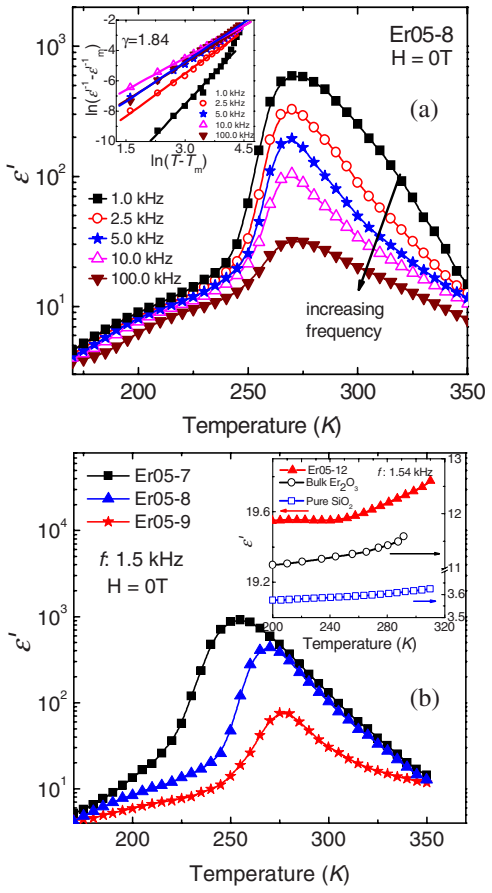

FIG. 2. (Color online) (a) The $(\varepsilon'-T)$ curves of Er05–8 at different frequency, inset: representative plots of $\ln(\varepsilon'^{-1}-\omega_m'^{-1})$ vs $\ln(T-T_m)$ at temperatures higher than T_m for the Er05–8 at different frequency values, (b) $(\varepsilon'-T)$ curves at different calcined temperatures, inset: $(\varepsilon'-T)$ curves of Er05–12, pure bulk Er_2O_3 (Ref. 31) and pure SiO_2 glass samples indicating low dielectric constant with non-DPT feature.

C. Dielectric relaxation analysis

To shed more light on the role of the relaxation dynamics, Fig. 3(a) depicts the temperature dependence of the dielectric

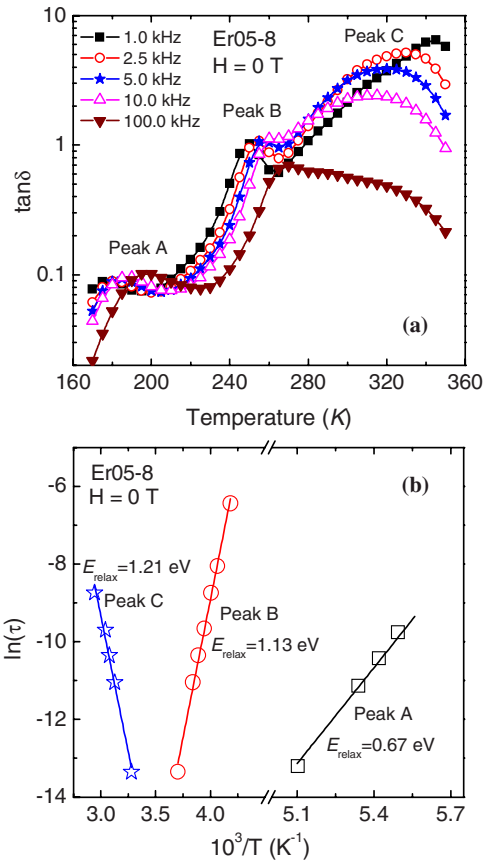

FIG. 3. (Color online) (a) Dielectric loss tan δ of Er05–8 at different frequency, (b) Representative Arrhenius plot of the relaxation time of Er05–8. The calculated activation energy values (in electron volt) are illustrated in each case.

loss tangent, tan δ for various frequencies. The main feature observed is the appearance three maxima (peak $A \sim 180$ K, peak $B \sim 260$ K, and peak $C > 320$ K) of tan δ-T. The former two shift to higher temperatures as the frequency is increased while the peak C with high-dielectric leakage (~ 7) is shifted to lower temperature with increasing frequency. The intensity of peak A is weaker (~ 0.15) than that of the other peaks at high temperatures. The most important outcome of this analysis is complemented by reading off loss-peak positions in the frequency and temperature-dependent plot. In Fig. 3(b), the resulting temperature dependence of τ is shown in an Arrhenius representation. Near the DPT temperature (T_m), thermally activated behavior, $\tau = \tau_o \exp(E_{relax}/kT)$, is observed with an energy barrier E_{relax} of about 1.13 eV. However, above 300 K, the temperature dependence of τ becomes reversed with activation energy 1.21 eV. These experimental facts suggest that the dielectric relaxation process might be closely associated with the presence of thermally activated oxygen vacancies. Thermally activated reorientation of dipole moment via the vacancy jumping (or, more correctly, the oxygen ion jumping through the oxygen vacancy) was also suggested earlier as the origin of the dielectric relaxation with activation energy $\sim 0.7-1.2$ eV.[33,34] Our present results support the recent experimental finding[34] that electrical properties of perovskite-type ABO_3 material are closely related to crystal structure and oxygen vacancies, which can be controlled by sintering process. The ε' value along with DPT behavior diminishes with reduced concentration of oxygen vacancies by annealing the sample at higher temperature. In addition, the possibility of the contact between the electrodes and sample influencing the dielectric properties is excluded by using different thickness of the samples and with different electrode materials. In both cases dielectric constant changes are found to be within experimental errors indicating intrinsic nature of this system.

D. Dielectric polarization studies

To check the possible ferroelectriclike (FEL) correlation in the sample, we studied the P-E curve with different experimental conditions (frequency and temperature dependence) and observed hysteresis loop shown in Fig. 4. The relatively narrow P-E loop near T_m (~ 270 K) without saturation (remnant polarization $P_r \sim 0.032$ μC/cm^2, and coercive field $E_c \sim 0.78$ kV/cm) demonstrates a noncanonical FEL behavior, similarly to that observed earlier in ABO_3 perovskites.[35] It is noted that this NP-glass composite (0.5 mol % Er_2O_3: 99.5 mol % SiO_2) system, the NP Er_2O_3 concentration is very small with very small dipole moment per unit volume and hence better structure of the loop might not be observed. The P-E curves look very much like those of a lossy dielectric-"banana loops," the terminology recently coined by Scott.[36] The hysteresis loops is slightly fatter at lower frequency. However, the P-E characteristics are also studied at different temperatures using higher polarization frequency (2.0 kHz), the maximum frequency limit of our instrument (Precision LC meter, Radiant Technologies). Because the high-frequency hysteresis loop would be more closely related to the intrinsic ferroelectric switching processes than the low-frequency counterpart.[37] Though the results of hysteresis loop becoming more pronounced with decreasing temperature from 320 to 275 K suggest ferroelectriclike ordering in Er05–8, the system is not purely ferroelectric for which further experiments are still necessary.

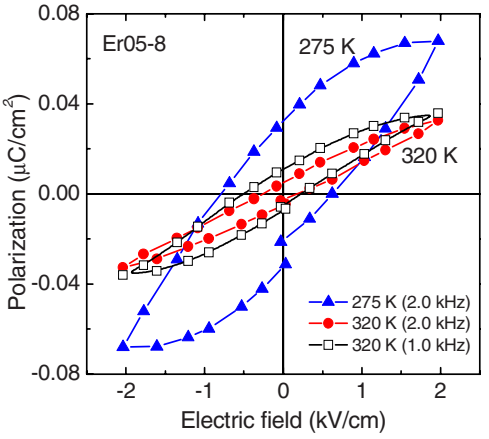

FIG. 4. (Color online) Dielectric hysteresis loop of Er05–8, measured near DPT (~ 275 K) and above room temperature (320 K) using 2.0 and 1.0 kHz polarization frequency.

E. Equivalent circuit analysis

It is well known that Maxwell-Wagner (MW) effect, or interfacial phenomena is usually adopted to explain the dielectric relaxation with high permittivity. The present NP-glass composite system consisting basically a mixture of magnetic NP Er_2O_3 grain separated by more insulating intergrain (SiO_2 matrix). Such an increase in the dielectric constant with DPT behavior might be a signature of the effect of internal barrier layer capacitance, which is directly proportional to the ratio of the grain size and the grain-boundary thickness. The impedance data have also been analyzed using an equivalent circuit consisting of two parallel resistor-capacitor (RC) elements connected in series (inset of Fig. 5). One RC element corresponds to the conducting region (Er_2O_3 NPs) and the other corresponds to the more resistive part (SiO_2 matrix) of the sample. Each RC element generally gives rise to an arc in the complex impedance Z''-Z' plane. The impedance spectroscopic data are analyzed with the help of commercial software (Z-VIEW, version 2.9c). According to the popular technique of explaining impedance spectra in the complex Z''-Z' plane, the high-frequency arc is assigned to the grain (intrinsic effect). Interestingly, at low temperature ($T_m < 270$ K) almost the entire measured frequency region ($20-2 \times 10^6$ Hz) is dominated by the grain response, governed by the intrinsic effect. The contribution of grain (Er_2O_3) resistance (R_g, values obtained from equivalent circuit model) with magnetic field effect is discussed in the next section.

F. Magnetodielectric effect

Another very interesting finding with this Er05–8 system is the observation of colossal MD effect as shown in Fig.

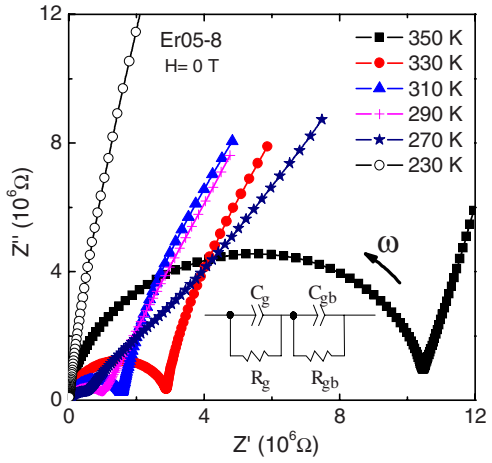

FIG. 5. (Color online) Complex plane plots, Z''-Z', of Er05–8 at several temperatures. The inset shows schematic model of equivalent electrical circuits.

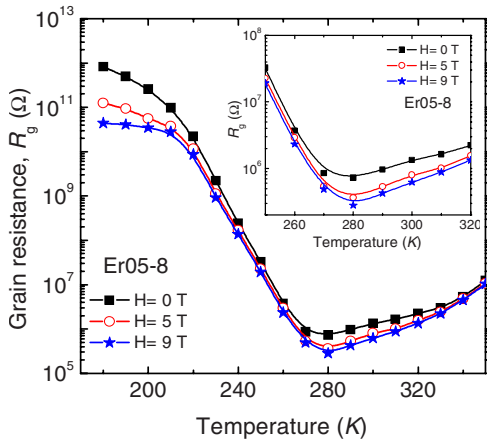

FIG. 7. (Color online) Temperature dependence of grain resistance (R_g) calculated from impedance complex plane plots with external magnetic field. Inset: The region close to T_m is highlighted.

6(a). A large increase in ε' (~2.75 times) under a magnetic field of 9 T is observed around the transition regime 260–300 K at a frequency of 2.5 kHz. The field dependent inverse of dielectric constant with temperature [upper inset of Fig. 6(a)] is also found to fit the Curie-Weiss law with Curie constant and Curie-Weiss temperature (T_o) as shown in Table I. It is

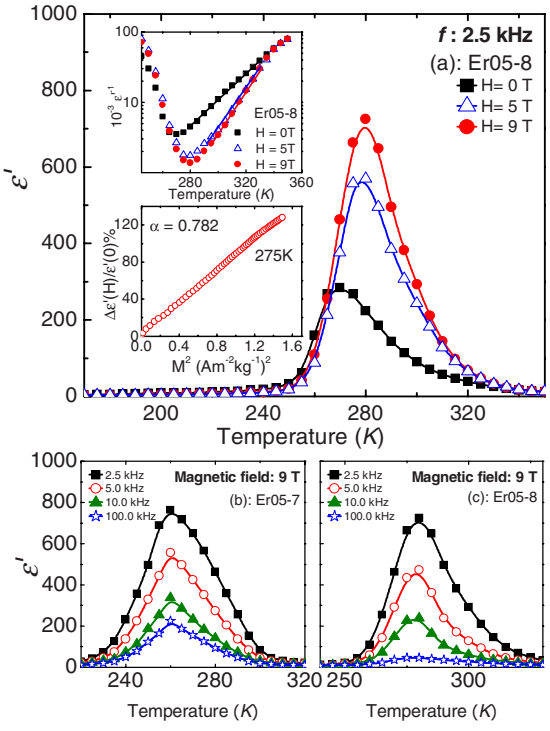

FIG. 6. (Color online) (a) The ($\varepsilon'-T$) curves of Er05–8 measured under different applied magnetic fields at a fixed frequency 2.5 kHz. Upper inset of (a): variation in the inverse ε' with temperature (exhibiting the Curie-Weiss behavior) and the lower inset of (a): dielectric strength ($\Delta\varepsilon'/\varepsilon'$) of Er05–8 showing linear variation with the square of magnetization M^2, measured in the vicinity of T_m (~275 K). [(b) and (c)] ($\varepsilon'-T$) curves of Er05–7 and Er05–8 measured with several frequencies under 9 T applied magnetic field.

noteworthy that both dielectric peak temperatures T_m and T_o shift to higher temperatures with increasing magnetic field. This indicates magnetic spin ordering occurs at higher temperature under magnetic field and hence spin-lattice coupling strength is reduced under magnetic field. Temperature and frequency-dependent dielectric constant measured at a typical higher magnetic field (~9 T) for two samples (Er05–7 and Er05–8) annealed at different temperatures are shown in Figs. 6(b) and 6(c). It is obvious from these figures that ε' value is larger in the lower temperature annealed sample (indicating particle size-dependent field effect of ε').[38] The system in which we observed MD effect (also showing Curie-Weiss behavior) is the single phase amorphous system (700–900 °C calcined samples where NPs of 2–10 nm of Er_2O_3 are formed). To further clarify the character of the MD effect, we have estimated the field dependent MD strength defined by $\{\Delta\varepsilon'(H)/\varepsilon'(0)=[\varepsilon'(H)-\varepsilon'(0)]/\varepsilon'(0)\}$ as a function of the square of the magnetization near T_m (~275 K) as shown in the lower inset of Fig. 6(a). Strikingly, this behavior can be well approximated by the scaling function, $\Delta\varepsilon'/\varepsilon' \approx \alpha M^2$ ($\alpha \sim 0.782$ is related to the magnetoelectric interaction constant and magnetostriction effect). Similar behavior is also observed in multiferroic $BiMnO_3$.[3] This result suggests that the dielectric properties of magnetic NPs in SiO_2 glass network are closely related to the disposition of the magnetic moments in the system. Thus in the present system, the MD effect is related to the magnetism, typical size and concentration of the amorphous NPs of the guest oxide (Er_2O_3) in the host SiO_2 glass.

Figure 7 shows the contribution of grain (amorphous NP Er_2O_3) resistance [R_g, extracted from equivalent circuit element (inset of Fig. 5)] of Er05–8 as a function of measuring temperature in presence of external magnetic field. Figure 8 demonstrates the temperature dependence of ac conductivity (σ_{ac}) at various frequencies. Temperature-dependent ac conductivity in presence of external magnetic field are plotted in inset of Fig. 8. Concomitantly, $R_g(T)$ (Fig. 7) reveals a metal to insulator like transition coinciding with the T_m of $\varepsilon'(T)$ [Fig. 2(a)] as well as $\sigma_{ac}(T)$ (Fig. 8) and interestingly the R_g decreases under magnetic field as in colossal magnetoresis-

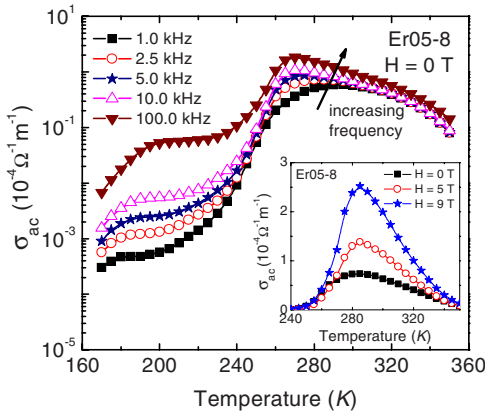

FIG. 8. (Color online) Temperature dependence of ac conductivity (σ_{ac}) of Er05–8 for various frequencies. Inset: temperature dependence of ac conductivity (σ_{ac}) at 2.5 kHz with external magnetic fields.

tive materials.[28] These experimental results imply that the nature of charge carries responsible for dielectric relaxation peaks and dc conduction belongs to the same category. It indicates that the polarization relaxation has a close relation with the conductivity in grain interior, and the polarization process depends on the conductivity of the charge in the grain interior.

It has been established that magnetic NPs often show magnetoresistive properties,[39] attributed to spin-polarized tunneling. Although we have investigated strong positive magnetoelectric interaction constant ($\alpha \sim 0.782$), it appears that the observed MD effect is caused essentially through the combination of magnetoresistance and above mentioned MW effect, as recently predicted by Catalan.[40] This MD behavior is strongly associated with magnetoresistance changes, depending on the NP size and separation. While the NP Er_2O_3 resistance decreases with the increase in external magnetic field, i.e., negative magnetoresistance, the dielectric constant increases with the increase in the external magnetic field, i.e., positive MD effect. The negative magnetoresistance and positive MD effect indicate that the superexchange-type interaction exists between the magnetic spin in the present system. Enhancement of MD effect through the resistance ratio might imply the possible tunability of the resistive MD effect. The amorphous NP $Er_2O_3:SiO_2$ arises spontaneously (self-organized) in a natural way with almost equal size and separation. The observation demonstrates the effect between magnetic and dielectric properties of NPs is apparently an intrinsic feature of this new family and independent of sample dimension. Moreover, the particle size, separation and concentrations of the Er_2O_3 NP contributing to the magnetically and electrically responded permittivity are easily controllable with annealing temperature/doping concentration. This amorphous NP-glass composite system may be the promising high-k gate dielectrics due to its high dielectric constant with MD effect, single-stage process in air at moderate temperature and good compatibility with modern microelectronics processing technique. Interestingly, as the particle size increases by annealing, DPT behavior and hence the associated MD effect decreases and ultimately dielectric constant become equal to be their bulk crystalline counterparts as in Er05–12 (with grain size >40 nm). This finding cannot, however, be classified by aforementioned MW contribution. An alternative possibility, the experimental facts strongly evidence that the dielectric anomaly with DPT behavior is related to oxygen-vacancy-induced dielectric relaxation. Other ABO_3-type oxides[34,41] were investigated with similar temperature-dependent behaviors, which reveal that the oxygen vacancy must be the basic reason attributed to the temperature-dependent diffuse ferroelectriclike properties. Returning to the dielectric relaxation in the $Er_2O_3:SiO_2$ NP-glass composite system, one may conclude that both the MW mechanism and the reorienting dipole-center model can explain the main features of colossal room-temperature MD response. However, further research is needed to establish that such rare-earth oxide NP embedded oxide glasses showing MD behavior is related to oxygen vacancies and magnetoresistive effect.

IV. CONCLUSION

In conclusion, it has been possible to synthesize Er_2O_3 NPs embedded in silica glass matrix by a sol-gel method. The NP Er_2O_3 in the glass SiO_2 matrix is formed spontaneously (self-organized) in a natural way with almost equal size and separation which can be tuned by calcination temperature and Er_2O_3 concentration, respectively. Properly annealed sol-gel glass shows an interesting colossal enhancement of dielectric constant associated with MD behavior around room temperature. The MD behavior is only observed in the $Er_2O_3:SiO_2$ glassy phase with amorphous Er_2O_3 NPs <10 nm. Such colossal MD effect is discussed in the context of the magnetic spin and the dipole coupling through the lattice, a direct consequence of exploiting magnetoresistance changes associated with NP size and concentration. Observed conduction mechanism is found to be closely related to the thermally activated oxygen vacancies. However, present study also stimulates further investigation with different rare-earth systems with different concentration to throw more light exploring the origin and application feasibility on these rich dielectric materials.

ACKNOWLEDGMENT

This work was supported by National Science Council, Taiwan under Grant No. NSC 97-2112-M-110-005-MY3.

*Permanent address: Department of Solid State Physics, Indian Association for the Cultivation of Science, Jadavpur, Kolkata 700 032, India.
†Corresponding author; yang@mail.phys.nsysu.edu.tw

[1] W. Eerenstein, N. D. Mathur, and J. F. Scott, Nature (London) **442**, 759 (2006).
[2] J. F. Scott, Science **315**, 954 (2007).
[3] T. Kimura, S. Kawamoto, I. Yamada, M. Azuma, M. Takano, and Y. Tokura, Phys. Rev. B **67**, 180401(R) (2003).
[4] J. Wang *et al.*, Science **299**, 1719 (2003).
[5] A. Sundaresan, R. V. K. Mangalam, A. Iyo, Y. Tanaka, and C. N. R. Rao, J. Mater. Chem. **18**, 2191 (2008).
[6] W. Eerenstein, F. D. Morrison, J. Dho, M. G. Blamire, J. F. Scott, and N. D. Mathur, Science **307**, 1203 (2005).
[7] J. Lu, J. Aarik, J. Sundqvist, K. Kukli, A. Hårsta, and J. O. Carlesson, J. Cryst. Growth **273**, 510 (2005).
[8] Z. J. Yan, R. Xu, Y. Y. Wang, S. Chen, Y. L. Fan, and Z. M. Jiang, Appl. Phys. Lett. **85**, 85 (2004).
[9] M. Copel, M. Gribelyuk, and E. Gusev, Appl. Phys. Lett. **76**, 436 (2000).
[10] L. Q. Zhu, Q. Fang, G. He, M. Liu, and L. D. Zhang, Nanotechnology **16**, 2865 (2005).
[11] G. B. Alers, R. M. Fleming, Y. H. Wong, B. Dennis, A. Pinczuk, G. Redinbo, R. Urdahl, E. Ong, and Z. Hasan, Appl. Phys. Lett. **72**, 1308 (1998).
[12] T. M. Klein, D. Niu, W. S. Epling, W. Li, D. M. Maher, C. C. Hobbs, R. I. Hegde, I. J. R. Baumvol, and G. N. Parsons, Appl. Phys. Lett. **75**, 4001 (1999).
[13] G. Lippert, J. Dąbrowski, V. Melnik, R. Sorge, C. Wenger, P. Zaumseil, and H.-J. Mussig, Appl. Phys. Lett. **86**, 042902 (2005).
[14] R. L. Nigro, R. G. Toro, G. Malandrino, V. Raineri, and I. L. Fragalà, Adv. Mater. **15**, 1071 (2003).
[15] D. Ceresoli and D. Vanderbilt, Phys. Rev. B **74**, 125108 (2006).
[16] K. J. Hubbard and D. G. Schlom, J. Mater. Res. **11**, 2757 (1996).
[17] V. V. Shvartsman, S. Bedanta, P. Borisov, W. Kleemann, A. Tkach, and P. M. Vilarinho, Phys. Rev. Lett. **101**, 165704 (2008).
[18] G. Lawes, R. Tackett, B. Adhikary, R. Naik, O. Masala, and R. Seshadri, Appl. Phys. Lett. **88**, 242903 (2006).
[19] R. Mazumder *et al.*, J. Appl. Phys. **100**, 033908 (2006).
[20] J. Blanusa, B. Antic, A. Kremenovic, A. S. Nikolic, L. Mazzerolles, S. Mentus, and V. Spasojevic, Solid State Commun. **144**, 310 (2007).
[21] M. Losurdo *et al.*, Adv. Funct. Mater. **17**, 3607 (2007).
[22] S. Chen, Y. Y. Zhu, R. Xu, Y. Q. Wu, X. J. Yang, Y. L. Fan, F. Lu, and Z. M. Jiang, Appl. Phys. Lett. **88**, 222902 (2006).
[23] S. Mukherjee, A. K. Pal, S. Bhattacharya, and J. Raittila, Phys. Rev. B **74**, 104413 (2006).
[24] M. Nogami and Y. Moriya, J. Non-Cryst. Solids **37**, 191 (1980).
[25] D. M. Krol and J. G. van Lierop, J. Non-Cryst. Solids **63**, 131 (1984).
[26] C. P. Sun, C. C. Lin, J. L. Her, C. J. Ho, S. Taran, H. Berger, B. K. Chaudhuri, and H. D. Yang, Phys. Rev. B **79**, 214116 (2009).
[27] JCPDF (Card No. 431007).
[28] J. Rivas, J. Mira, B. Rivas-Murias, A. Fondado, J. Dec, W. Kleemann, and M. A. Senarí-Rodríuez, Appl. Phys. Lett. **88**, 242906 (2006).
[29] A. Jana, T. K. Kundu, S. K. Pradhan, and D. Chakravorty, J. Appl. Phys. **97**, 044311 (2005).
[30] I. Rivera, A. Kumar, N. Ortega, R. S. Katiyar, and S. Lushnikov, Solid State Commun. **149**, 172 (2009).
[31] H. B. Lal, J. Phys. C **13**, 3969 (1980).
[32] Z. Yu, C. Ang, R. Guo, and A. S. Bhalla, J. Appl. Phys. **92**, 2655 (2002).
[33] O. Raymond, R. Font, N. Suárez-Almodovar, J. Portelles, and J. M. Siqueiros, J. Appl. Phys. **97**, 084107 (2005).
[34] C. Ang, Z. Yu, and L. E. Cross, Phys. Rev. B **62**, 228 (2000).
[35] G. A. Samara, J. Phys.: Condens. Matter **15**, R367 (2003).
[36] J. F. Scott, J. Phys.: Condens. Matter **20**, 021001 (2008).
[37] L. Pintilie and M. Alexe, Appl. Phys. Lett. **87**, 112903 (2005).
[38] S. Yáñez-Vilar, J. Mira, M. Sánchez-Andújar, S. Castro-García, A. Fondado, J. Rivas, and M. A. Senarís-Rodríguez, Appl. Phys. Lett. **96**, 162904 (2010).
[39] J. Tang, L. Feng, and J. A. Wiemann, Appl. Phys. Lett. **74**, 2522 (1999).
[40] G. Catalan, Appl. Phys. Lett. **88**, 102902 (2006).
[41] G. Y. Yang, E. C. Dickey, and C. A. Randall, J. Appl. Phys. **94**, 5990 (2003).